Molecular Magnetism

International Edition: DOI: 10.1002/anie.201510468
German Edition: DOI: 10.1002/ange.201510468

Rotating Magnetocaloric Effect in an Anisotropic Molecular Dimer

*Giulia Lorusso, Olivier Roubeau, and Marco Evangelisti**

Abstract: *In contrast to the mainstream research on molecular refrigerants that seeks magnetically isotropic molecules, we show that the magnetic anisotropy of dysprosium acetate tetrahydrate, $[\{Dy(OAc)_3(H_2O)_2\}_2]\cdot 4H_2O$ (**1**), can be efficiently used for cooling below liquid-helium temperature. This is attained by rotating aligned single-crystal samples in a constant applied magnetic field. The envisioned advantages are fast cooling cycles and potentially compact refrigerators.*

Gadolinium is the most widespread magnetic element among molecular refrigerant materials.[1] It occupies this position because isotropic spins facilitate the occurrence of a large change of the magnetic entropy and adiabatic temperature following a change in the applied magnetic field, that is, the magnetocaloric effect (MCE).[2] Nonetheless, magnetic anisotropy can play in favor when exploited properly. In any typical cryogenic adiabatic demagnetization refrigerator (ADR), the cooling process proceeds by removal of a magnetic field (B), which is applied by making use of a superconducting magnet. Ideally, one would like to sweep the field very fast in order to minimize irreversible heat flows and facilitate temperature stabilization.[3] The operation time for the full removal of B, the strength of which is a few teslas, is limited by the magnet to be of the order of minutes. However, the use of anisotropic magnetocaloric materials can provide an opportunity for reducing this operation time down to the order of seconds. This can be attained by rotating well-oriented single crystals of an anisotropic magnetocaloric material in a constant applied magnetic field,[4] as experimentally investigated for $HoMn_2O_5$ and $KEr(MoO_4)_2$.[5,6] In fact, the MCE of anisotropic magnetic materials varies depending on the orientation of B.[7] Therefore, a controlled rotation of the functional material in constant B can lead to a temperature change, the sign of which depends on the direction of the circular motion (Figure 1).

The magnetocaloric properties of molecular compounds have largely been explored.[1] The vast majority of molecular refrigerants are excellent candidates for temperatures between 1 and 10 K, for which their MCE can be larger than that of conventional magnetic refrigerants. Since the report on lanthanide-based calix[4]arene clusters,[8] the methodology usually adopted is that of studying spin-lattice relaxation phenomena for the analogs based on anisotropic lanthanide ions, whilst leaving MCE investigations only for the magnetically isotropic Gd^{3+} analog. Publications on the anisotropic MCE of molecule-based compounds are very seldom encountered,[9,10] and with good reasons.[2] In contrast to this trend, we here present the first study on the rotating anisotropic MCE for a molecular compound, namely dysprosium acetate tetrahydrate, $[\{Dy(OAc)_3(H_2O)_2\}_2]\cdot 4H_2O$ (**1**, Figure 2a)[11,12]—its Gd^{3+} analog (**2**) was already shown to be an excellent and versatile magnetic refrigerant.[13,14] The crystal-field anisotropy in the Dy^{3+} ion, the ground state of which is $^6H_{15/2}$ ($4f^9$, $J=15/2$, $S=5/2$, $L=5$, $g_J=4/3$), plays the crucial part in determining the magnetic properties.[15] Our measurements show that, for instance, starting from the normal boiling temperature of ^{4}He (4.2 K) and in a static field of 5 T, single-crystal samples of **1** cool down to 2 K, following a single 90°-rotation that changes the orientation of B from being perpendicular to the crystallographic bc plane to parallel to the c axis. Similar temperature gradients are routinely attained by pumping liquid helium. Our results suggest that, by substituting the rotary pump, a compact and efficient refrigerator based on the rotating anisotropic MCE can potentially be implemented.

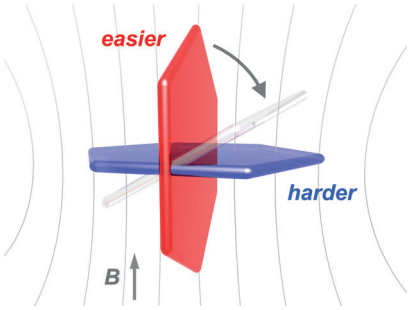

Figure 1. The magnetically anisotropic single crystal decreases its temperature following a rotation from an easier to a harder magnetization direction in constant applied magnetic field. Within the same configuration, the single crystal increases its temperature following a rotation from a harder to an easier magnetization direction.

Single crystals of **1** are obtained in high yield by warming dysprosium oxide in a water-acetic acid mixture (see the Supporting Information for details). At room temperature, the compound is isostructural to the Gd analog and other intermediate lanthanides[11,16] and crystallizes in the triclinic $P\bar{1}$ space group as a dimeric neutral molecule with two $\eta^2{:}\eta^1{:}\mu_2$-carboxylate bridges and a Dy···Dy separation of 4.173 Å (Figure 2a). In the crystal, the molecules of **1** are interacting in the ab plane through direct intermolecular H bonds of their terminal H_2O, while interplane hydrogen bonds involve the lattice H_2O molecules. We have also determined the structure of **1** at 30 K, closer to the temper-

[*] Dr. G. Lorusso, Dr. O. Roubeau, Dr. M. Evangelisti
Instituto de Ciencia de Materiales de Aragón (ICMA)
CSIC—University of Zaragoza
50009 Zaragoza (Spain)
E-mail: evange@unizar.es

Supporting information, including the full experimental details for the synthesis and characterization of the reported compound, and ORCID(s) from the author(s) for this article are available on the WWW under http://dx.doi.org/10.1002/anie.201510468.

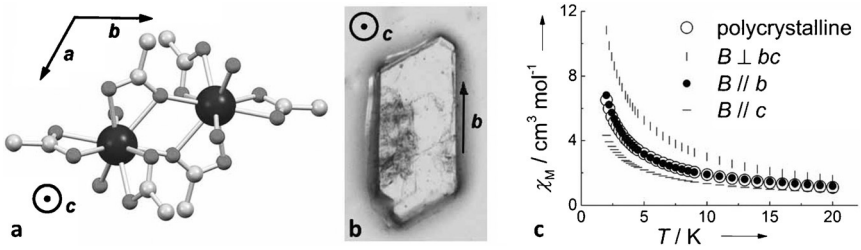

Figure 2. a) Molecular structure of **1**, b) photograph of a typical single-crystal sample, and c) temperature-dependence of the experimental molar susceptibility for a polycrystalline (empty dots) and single-crystal (filled dots) sample of **1**, for an applied field $B = 0.1$ *T*, oriented along the three directions indicated. Crystallographic axes are highlighted. Dy = black, O = dark gray, C = light gray. H atoms and lattice water molecules are omitted for clarity.

atures of interest for MCE.[17] No significant modifications of the structure are observed, besides the expected thermal contraction. The cell volume is reduced by 2.5 % at 650.59 Å^3, while the intra- and shortest intermolecular Dy···Dy separations are now 4.135 and 6.157 Å, respectively. Well-shaped large single crystals tend to show a six-sided elongated thick platy habit, with the longer crystal direction coinciding with the crystallographic *b* axis and the large flat surface perpendicular to the crystallographic *c* axis—the corresponding α angle is indeed close to 90°, being 91.71° and 92.09°, respectively, at 293 and 30 K (see Figure 2b). The crystallographic *a* axis is along the third side/direction of the crystals but not strictly parallel to it as it forms a close to 120° angle with the *c* axis, being 117.88 and 118.33°, respectively, at 293 and 30 K.

Magnetization measurements are performed on polycrystalline and single-crystal samples of **1**. For a polycrystalline sample, the product of the direct current (dc) molar susceptibility with the temperature ($\chi_M T$; see Figure S2 in the Supporting Information) agrees with previous studies.[12] This compound exhibits paramagnetism and no zero-field out-of-phase alternating current (ac) susceptibility, at least down to 2 K (not shown here). Single-crystal measurements are conducted for *B* applied along three directions in the crystallographic referential frame, which are dictated by the main growth directions of the crystals (Figure 2). Specifically, these directions are for *B* applied perpendicular to the crystallographic *bc* plane, and parallel to the crystallographic *b* and *c* axes, respectively. Figure 2c shows that the low-*T* χ_M depends significantly on the direction considered, that is larger values are attained for $B \perp bc$ and lower ones for $B//c$, denoting them as easier and harder magnetization directions, respectively. The polycrystalline sample yields a low-temperature χ_M which is intermediate between the signals for the two aforementioned directions, and close to the χ_M collected for $B//b$ (Figure 2c).

For a polycrystalline sample of **1**, we collected isothermal magnetization (*M*) and specific heat (*C*) data (see Figures S2 and S3 in the Supporting Information, respectively). From *C*, we calculate the entropy $S(T,B) = \int_0^T C(T',B)/T' \, dT'$. The zero-applied-field *T*-dependent *C* comprises two well-separated magnetic contributions, as typically encountered for Dy^{3+}-based complexes.[18] For temperatures approximately between 3 and 20 K, a broad magnetic bump, associated to crystal-field splitting, develops concomitantly with the predominant nonmagnetic lattice specific heat. On lowering the temperature below 2–3 K, a field-dependent feature increases as $C \propto T^{-2}$, denoting the onset of a magnetic anomaly. On basis of the associated entropy content (see Figure S3 in the Supporting Information), we note that only the lowest doublet is occupied at these low temperatures, thus implying an effective spin 1/2 as the ground state. Therefore, the experimental *C* below 2–3 K can be well-described by a two-level Schottky anomaly, yielding an energy splitting $\Delta \approx 0.8$ K, equivalent to a local field of $B_{loc} \approx 0.6$ T, likely associated to a large extent to the $Dy^{3+}\cdots Dy^{3+}$ intramolecular superexchange interaction.

A full evaluation of the MCE implies determining the change of the magnetic entropy (ΔS_m) and adiabatic temperature (ΔT_{ad}), both as a function of *T*, following a change of the applied magnetic field $\Delta B = B_i - B_f$ (see Supporting Information, Figure S4 for the definition of MCE). In terms of the MCE, compound **1** in its polycrystalline form is not significantly interesting, especially when compared with the magnetically-isotropic **2**. From the $S(T, B)$ data, we obtain the magnetic entropy change for $\Delta B = B_i - B_f = (3-0)$ *T*, which is plotted in the Supporting Information, Figure S5. Note that the lattice contribution to *C*, hence *S*, is field-independent and, therefore, irrelevant for these calculations since it cancels out by subtracting between entropies. Furthermore, by applying the Maxwell equation to the magnetization data, $\Delta S_m(T, \Delta B) = \int_{B_i}^{B_f} (\partial M(T,B)/\partial T)_B dB$, the magnetic entropy change for $\Delta B = (3-0)$ *T* is obtained and depicted in Figure S5 in the Supporting Information together with the aforementioned calculation using the $S(T, B)$ data. The agreement between the two sets of data proves the validity of both approaches. For comparison, Figure S5 in the Supporting Information also shows the equivalent set of $\Delta S_m(T, \Delta B)$ data for **2**, obtained from ref. [13]. We observe that the MCE of the polycrystalline sample of **1** is smaller (roughly by 2/3) than that of **2**. This behavior is to be expected because the larger the magnetic anisotropy, the more pronounced are the crystal-field effects that, splitting the energy levels, result in broader and smaller MCE features at higher *T*.[2]

Next, we focus on the anisotropic MCE of **1**, the full determination of which includes *M* measurements for *B* oriented along the three directions selected (Figure S6) and *C* measurements for $B = 0$. Note that zero-applied field measurements of *C* provide identical results regardless of whether the sample is in the polycrystalline or single-crystal form (only the former set of data are shown in Figure S3). For the magnetization experiments and for each field orientation, we work with $B \leq 5$ T and $2 \text{ K} < T < 20$ K. As seen by comparing the results shown in Figure S6, the overall larger (smaller) *M* is achieved for $B \perp bc$ ($B//c$), validating this orientation as the relatively easier (harder).

Following the same procedure adopted for the polycrystalline sample of **1**, we apply the Maxwell equation to the M data collected for a single-crystal sample (Supporting Information, Figure S6). We obtain ΔS_m for **1** as a function of T, applied field change (ΔB) and orientation ($B \perp bc$, $B//b$ and $B//c$). For a proper evaluation of the anisotropic MCE, that is, for determining also ΔT_{ad}, we make use of the zero-field entropy data $S(T, 0)$ and note that simply $S(T, B) = S(T, 0) + \Delta S_m(T, \Delta B = B - 0)$, for any orientation of B. From the so-obtained $S(T, B)$, we calculate $\Delta T_{ad}(T, \Delta B)$, which is depicted together with $\Delta S_m(T, \Delta B)$ in Figure 3 for $B \perp bc$, $B//b$ and $B//c$. Note that we define the adiabatic temperature change as $\Delta T_{ad} = T_i - T_f$ for $\Delta B = B_i - B_f$ (see Figure S4) and adopt the convention that the T values in the abscissae of Figure 3 are the final temperatures, T_f, reached in the corresponding adiabatic cooling process. All data presented are limited by the lowest temperature (2 K) attained in the single-crystal M measurements.

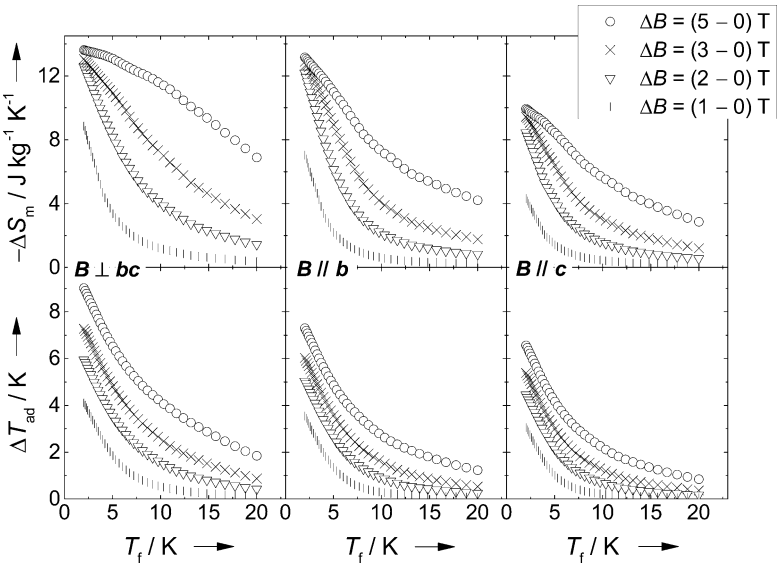

Figure 3. For a single crystal of **1**, temperature-dependence of the magnetic entropy change ΔS_m (top) and adiabatic temperature change ΔT_{ad} (bottom) for selected changes of the magnetic field, as labeled. From left to right, the magnetic field is oriented perpendicular to the crystallographic *bc* plane, parallel to the crystallographic *b* axis, and parallel to the crystallographic *c* axis, respectively.

From the C experiments, we have obtained indications on how the magnetic entropy is released as a function of temperature. Correspondingly, MCE maxima are attained for the lowest experimentally accessed T and, to a lesser extent, for the 10 K temperature region, as especially evident for $B \perp bc$ (Figure 3). As anticipated, the overall strength of the MCE diminishes with the increase of the anisotropy, being thus stronger for the easier direction, $B \perp bc$, reaching the maximum values $-\Delta S_m = 13.6\ J\,kg^{-1}K^{-1}$ and $\Delta T_{ad} = 9.0$ K at $T \simeq 2$ K and $\Delta B = (5-0)$ T. For $B//b$, $T \simeq 2$ K and $\Delta B = (5-0)$ T, the MCE maxima are $-\Delta S_m = 13.0\ J\,kg^{-1}K^{-1}$ and $\Delta T_{ad} = 7.3$ K. For $B//c$, $T \simeq 2$ K and $\Delta B = (5-0)$ T, the MCE maxima are $-\Delta S_m = 9.9\ J\,kg^{-1}K^{-1}$ and $\Delta T_{ad} = 6.5$ K. Note that the lower the anisotropy, the closer $-\Delta S_m(T, \Delta B)$ approaches the maximum entropy value per mole involved at these temperatures, that is, $14.0\ J\,kg^{-1}K^{-1}$ (see Figure S3). As expected, under similar experimental conditions, the strength of the MCE for the polycrystalline sample is in between these values (Figure S5), whilst all of them are significantly smaller than the corresponding ones for **2**.[13]

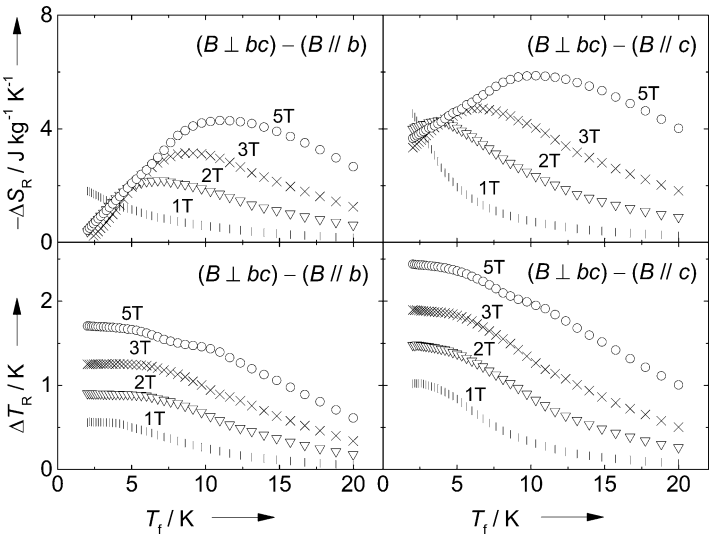

Figure 4. Temperature dependence of the magnetic entropy change ΔS_R (top) and adiabatic temperature change ΔT_R (bottom) resulting from rotating a single crystal of **1** by 90° from the $B \perp bc$ direction to either the $B//b$ (left) or $B//c$ (right) directions in constant magnetic fields, as labeled.

Finally, we have gathered all the information needed for evaluating the effect of rotating a single crystal of **1** in constant B. By differentiating between the data plotted in Figure 3, we determine the change in ΔS_m, that we denote as ΔS_R, and the change in ΔT_{ad}, that we denote as ΔT_R, associated with a certain rotation. Let us consider the following two 90° rotations in Figure 4: from $B \perp bc$ to $B//b$, that is, $\Delta S_R = \Delta S_m(B \perp bc) - \Delta S_m(B//b)$ and $\Delta T_R = \Delta T_{ad}(B \perp bc) - \Delta T_{ad}B//b$, and from $B \perp bc$ to $B//c$, that is, $\Delta S_R = \Delta S_m(B \perp bc) - \Delta S_m(B//c)$ and $\Delta T_R = \Delta T_{ad}(B \perp bc) - \Delta T_{ad}(B//c)$. The latter rotation yields an overall stronger effect, since it implies a larger change of the magnetic anisotropy. For both rotations, the T-dependence of ΔS_R varies significantly with the strength of B. The behavior of ΔT_R is more indicative for assessing the performance of this material as an anisotropic magnetic cooler. Figure 4 shows that ΔT_R attains its maximum value at the experimentally lowest investigated temperature, that is, $T_f = 2$ K, where T_f is the final temperature reached by the single crystal after the rotation. To facilitate the interpretation, we equivalently express the T gradients plotted in Figure 4 as function of the initial temperature ($T_i = \Delta T_R + T_f$) of the single crystal before the rotation (Figure S7). For example, ΔT_R is ca. 2.5 K when

the single crystal is rotated at $T_i = 4.5$ K from $B \perp bc$ to $B//c$, without changing $B = 5$ T.

Cooling by rotation requires magnetic anisotropy. The inherent drawback is that the overall strength of the MCE diminishes, the more so the stronger the anisotropy,[2] impacting negatively on, for example, the refrigerant capacity ($\propto \int |\Delta S_m| dT$).[19] This is made evident by comparing the MCE of **1** and **2**. For delivering the same refrigerant capacity, a conventional ADR would roughly require a three-times larger amount of **1**, with respect to **2** (see Figure S5). A relatively more massive ADR would imply slower operations, hence worse thermalization and dissipation. However, cooling by rotation also requires a properly redesigned magnetic refrigerator, a cryogenic roto-cooler, which is capable of exploiting the anisotropic MCE.[20] In principle, such device is relatively simple to implement. Importantly, it would guarantee fast cycling times for the cooling process and, by so-doing, also a comparatively better T stabilization and lower heat-dissipation than a conventional ADR. Therefore, the choice of which approach to follow has to be assessed not exclusively on basis of the magnetocaloric properties but also on the characteristics of the targeted application.

We expect that molecular compounds with a larger magnetic anisotropy than **1** should yield a correspondingly larger rotating anisotropic MCE. However, this enhancement should also be accompanied by an increase of the temperature at which the effect has its maximum strength. In this respect, the sizeable yet not exceptionally large magnetic anisotropy of **1** makes this material particularly appealing because the resulting ΔT_R takes place at temperatures technologically relevant, such as those (5 K) covered by conventional magnetic refrigeration and pumped helium. One could foresee the substitution of rotary pumps, which are routinely employed for attaining these T gradients in multi-stage refrigerators operating with liquid helium or a 4 K cryocooler. As already pointed out, the envisioned advantage is a potentially compact refrigerator either based on a large enough single crystal or an aggregate of oriented single crystals of this material.

Acknowledgements

We are grateful to Spanish MINECO for financial support (grand number FEDER-MAT2012-38318-C03-01) and for a postdoctoral contract (to G.L.), as well as to Dr. K. J. Gagnon for his help with the 30 K structural study. The Advanced Light Source is supported by the Director, Office of Science, Office of Basic Energy Sciences, of the U.S. Department of Energy under contract number DE-AC02-05CH11231.

Keywords: cryogenics · dysprosium · magnetocaloric effect · molecular magnetism · molecular refrigerants

How to cite: *Angew. Chem. Int. Ed.* **2016**, *55*, 3360–3363
Angew. Chem. **2016**, *128*, 3421–3424

[1] a) For a recent overview, see, for example, J. W. Sharples, D. Collison, *Polyhedron* **2013**, *54*, 91–103, and references therein; b) J. W. Sharples, D. Collison, E. J. L. McInnes, J. Schnack, E. Palacios, M. Evangelisti, *Nat. Commun.* **2014**, *5*, 5321.
[2] M. Evangelisti, E. K. Brechin, *Dalton Trans.* **2010**, *39*, 4672–4676.
[3] A. M. Tishin, Y. I. Spichkin, *The magnetocaloric effect and its applications (Series in Condensed Matter Physics)*, IOP, Bristol **2003**.
[4] P. J. von Ranke, N. A. de Oliveira, D. C. Garcia, V. S. R. de Sousa, V. A. de Souza, A. Magnus, G. Carvalho, S. Gama, M. S. Reis, *Phys. Rev. B* **2007**, *75*, 184420.
[5] M. Balli, S. Jandl, P. Fournier, M. M. Gospodinov, *Appl. Phys. Lett.* **2014**, *104*, 232402.
[6] V. Tkáč, A. Orendáčová, E. Čižmár, M. Orendáč, A. Feher, A. G. Anders, *Phys. Rev. B* **2015**, *92*, 024406.
[7] N. A. de Oliveira, P. J. von Ranke, *Phys. Rep.* **2010**, *489*, 89–159.
[8] G. Karotsis, S. Kennedy, S. J. Teat, C. M. Beavers, D. A. Fowler, J. J. Morales, M. Evangelisti, S. J. Dalgarno, E. K. Brechin, *J. Am. Chem. Soc.* **2010**, *132*, 12983–12990.
[9] X. X. Zhang, H. L. Wei, Z. Q. Zhang, L. Zhang, *Phys. Rev. Lett.* **2001**, *87*, 157203.
[10] P. J. Saines, J. A. M. Paddison, P. M. M. Thygesen, M. G. Tucker, *Mater. Horiz.* **2015**, *2*, 528–535.
[11] R. Baggio, J. C. Muñoz, M. Perec, *Acta Crystallogr. Sect. C* **2002**, *58*, m498–m500.
[12] Y.-Z. Zheng, Y. Lan, W. Wernsdorfer, C. E. Anson, A. K. Powell, *Chem. Eur. J.* **2009**, *15*, 12566–12570.
[13] M. Evangelisti, O. Roubeau, E. Palacios, A. Camón, T. N. Hooper, E. K. Brechin, J. J. Alonso, *Angew. Chem. Int. Ed.* **2011**, *50*, 6606–6609; *Angew. Chem.* **2011**, *123*, 6736–6739.
[14] G. Lorusso, M. Jenkins, P. González-Monje, A. Arauzo, J. Sesé, D. Ruiz-Molina, O. Roubeau, M. Evangelisti, *Adv. Mater.* **2013**, *25*, 2984–2988.
[15] D. Gatteschi, *Nat. Chem.* **2011**, *3*, 830.
[16] M. C. Favas, D. L. Kepert, B. W. Skelton, A. H. White, *J. Chem. Soc. Dalton Trans.* **1980**, 454–458.
[17] Crystallographic data for **1** are provided in the Supporting Information. CCDC 1433157 contains the supplementary crystallographic data for this paper. These data can be obtained free of charge from The Cambridge Crystallographic Data Centre via www.ccdc.cam.ac.uk/data_request/cif.
[18] S. Cardona-Serra, J. M. Clemente-Juan, E. Coronado, A. Gaita-Ariño, A. Camón, M. Evangelisti, F. Luis, M. J. Martínez-Pérez, J. Sesé, *J. Am. Chem. Soc.* **2012**, *134*, 14982–14990.
[19] M. E. Wood, W. H. Potter, *Cryogenics* **1985**, *25*, 667–683.
[20] M. D. Kuz′min, A. M. Tishin, *J. Phys. D* **1991**, *24*, 2039–2044.

Received: November 11, 2015
Published online: February 2, 2016

